Temperature and Redox Dual-Responsive Biodegradable Nanogels for Optimizing Antitumor Drug Delivery

ARTICLE *in* PARTICLE AND PARTICLE SYSTEMS CHARACTERIZATION · NOVEMBER 2015

Impact Factor: 3.08 · DOI: 10.1002/ppsc.201500153

6 AUTHORS, INCLUDING:

Shun Shen

Fudan University

49 PUBLICATIONS **690** CITATIONS

SEE PROFILE

Yajun Wang

Fudan University

38 PUBLICATIONS **1,439** CITATIONS

SEE PROFILE

Wuli Yang

Fudan University

154 PUBLICATIONS **4,586** CITATIONS

SEE PROFILE

Particle & Particle Systems Characterization
www.particle-journal.com

Temperature and Redox Dual-Responsive Biodegradable Nanogels for Optimizing Antitumor Drug Delivery

*Yefei Tian, Yang Wang, Shun Shen, Xinguo Jiang, Yajun Wang, and Wuli Yang**

The strategy to efficiently deliver antitumor drugs via nanocarriers to targeted tumor sites and achieve controllable drug release is attracting great research interest in cancer therapy. In this study, a novel type of disulfide-bonded poly(vinylcaprolactam) (PVCL)-based nanogels with tunable volume phase transition temperature and excellent redox-labile property are prepared. The nanogels are hydrophilic and swell at 37 °C, whereas under hyperthermia (e.g., 41 °C), the nanogels undergo sharp hydrophilic/hydrophobic transition and volume collapse, which enhances the cellular uptake and drug release. The incorporation of disulfide bond linkers endows the nanogels with an excellent disassembly property in reducing environments, which greatly facilitates drug release in tumor cells. Nanogels loaded with doxorubicin (DOX) (DOX-NGs) (DOX-NGs) are stable in physiological conditions with low drug leakage (15% in 48 h), while burst release of DOX (92% in 12 h) can be achieved in the presence of 10×10^{-3} M glutathione and under hyperthermia. The DOX-NGs possess improved cell killing efficiency under hyperthermia (IC_{50} decreased from 1.58 μg mL^{-1} under normothermia to 0.5 μg mL^{-1}). Further, the DOX-NGs show a pronounced tumor inhibition rate of 46.6% compared with free DOX, demonstrating that this new dual-responsive nanogels have great potential as drug delivery carriers for cancer therapy in vivo.

1. Introduction

During chemotherapy, the administration of free anticancer drugs shows lethal side effects for its nonspecific biodistribution and high cytotoxicity toward normal cells.[1] To achieve the ideal pharmacodynamics of anticancer drugs, nanocarrier drug delivery systems with a nanoscale size dimension (10–200 nm), stability in blood circulation, enhanced interaction with target cells, and controlled drug release manner are highly preferable.[2] One way to integrate the controlled drug release and selective drug delivery is the stimuli-responsive drug delivery systems, which are capable to undergo abrupt physicochemical changes in response to slight variation in external environmental variables, such as temperature,[3] pH,[4] redox potential,[5] and light.[6] Among various stimuli, temperature has gained more popularity in the application of drug delivery systems, because many pathological processes in various tissues are accompanied with local temperature increase by 1–5 °C.[7] This change of temperature can be utilized as a local drive to increase the cellular uptake or/and active the drug release inside the tumor tissue.[8] Thermoresponsive polymers exhibiting a reversible lower critical solution temperature (LCST) around the physiological temperature are the most common examples to fabricate temperature-responsive drug delivery systems, such as poly(*N*-isopropylacrylamide) (PNIPAM) and poly(*N*-vinylcaprolactam) (PVCL). These polymers undergo a sharp phase transition at their LCST, changing from hydrophilic coil below this temperature to a water-insoluble globule above it.[9] The nanoparticles with a hydrophilic surface can suppress their interaction with the cell membranes and proteins that ensures the long circulation, whereas the hydrophobic surface can accelerate the internalization of nanoparticles into cells by enhancing their adhesion to cell membranes.[8] Previous studies[10] have shown that the hydrophilic/hydrophobic switchable properties of thermoresponsive polymeric micelles composed of PNIPAM derivatives and hydrophobic segments could be used to control the cell adhesion/detachment behavior. Further, the structure change of polymeric micelles accompanying the phase transition could be used to control the drug release.[11]

Although thermoresponsive polymeric micelles have shown good performance in drug delivery systems for the combination of target drug delivery and controlled drug release, most of them have an unacceptably high critical micellization concentration and poor stability in blood that largely limits their application in clinical therapy.[12] To overcome these disadvantages, thermoresponsive nanogels formed by the crosslinking of temperature-responsive polymeric building blocks have been proposed as a more desirable platform for targeting drug

Y. Tian, Dr. Y. Wang, Prof. W. Yang
State Key Laboratory of Molecular Engineering of Polymers and Department of Macromolecular Science
Fudan University
220 Handan Road, Shanghai 200433, P. R. China
E-mail: wlyang@fudan.edu.cn
Dr. S. Shen, Prof. X. Jiang
School of Pharmacy & Key Laboratory of Smart Drug Delivery
Fudan University
826 Zhangheng Road, Shanghai 201203, P. R. China
Dr. Y. Wang
Department of Chemistry
Fudan University
220 Handan Road, Shanghai 200433, P. R. China

DOI: 10.1002/ppsc.201500153

delivery due to their excellent colloidal stability and precise control of the response toward temperature changes.[13] In nanogel form, the thermoresponse of PNIPAM and PVCL is manifested as a thermoinduced dramatic volume collapse during the hydrophilic/hydrophobic transition,[9b] which has been utilized for controlling the release of drugs.[14] Moreover, the volume phase transition temperature (VPTT) of thermoresponsive nanogels could be finely adjusted through the copolymerization of hydrophilic monomers.[15] However, the release of drugs induced by volume collapse can hardly achieve efficient release, additional functions such as triggered deconstruction of the nanogels are desirable.

To facilitate the release of loaded drugs and promote the physiologic clearance, cleavable cross-linkers are often incorporated to realize degradable polymeric carriers. Among various cleavable groups, disulfide bonds are of great interest for their characteristic degradation in response to physiologically relevant reducing conditions.[16] Drug delivery carriers incorporating disulfide bonds can undergo selective degradation upon entering the cytosol, in which the reducing glutathione (GSH) concentration (≈2–10 × 10^{-3} M) is much higher than that in the extracellular fluids.[17] In the last decades, disulfide bonds have been exploited in a wide variety of architectures, including micelles,[18] capsules,[19] and nanogels,[20] and proved to be a preferred means to construct biodegradable drug delivery systems.[16a]

Herein, PVCL-based nanogels were prepared through aqueous precipitation copolymerization of vinylcaprolactam (VCL) and *N*-(2-hydroxypropyl)methacrylamide (HPMA), as PVCL exhibits better biocompatible without unwanted neurotoxin as compared with PNIPAM (**Scheme 1**).[9a] The polymer chains were crosslinked by the disulfide-containing crosslinker *N,N′*-bis(acryloyl)cystamine (BAC) during the polymerization, which endows the nanogels with redox-labile property. These PVCL-based nanogels exhibit a sharp hydrophilic/hydrophobic transition and volume collapse at specific temperature. The VPTT of the nanogels was finely tailored in the range of 35–44 °C by varying the mass fraction of HPMA. In blood vessel (37 °C), the hydrophilic property of nanogel ensured its stable blood circulation. When reaching the tumor site, higher temperature of the tumor tissues caused nanogels to turn into hydrophobic state that enhanced the cell uptake of nanogels. Upon entering the tumor cells, a burst drug release occurs as a consequence of redox-triggered degradation of nanogels (Scheme 1). Through these dual-responsive nanocarriers, the target drug delivery and controlled drug release were simultaneously achieved. We believe the well-designed nanogels with temperature-sensitivity, redox-labile property, and adjustable VPTT could be a novel favorable platform for targeting drug delivery.

2. Results and Discussion

2.1. Preparation of Thermoresponsive P(VCL-*s*-*s*-HPMA) Nanogels

Here, the dual-stimuli responsive PVCL-based nanogels were prepared by aqueous precipitation copolymerization of VCL, HPMA, and disulfide-containing crosslinker. Aqueous precipitation polymerization is a simple one-pot method to prepare monodisperse nanospheres with no or thimbleful surfactants.[21] To optimize the temperature responsiveness, the neutral hydrophilic comonomer HPMA was incorporated in the polymer networks during polymerization. It has been shown that HPMA is high biocompatibility and nonimmunogenicity.[22] P(VCL-*s*-*s*-HPMA) nanogels with different HPMA content were fabricated, and the typical recipe and the mean hydrodynamic diameters (D_h) of a series of P(VCL-*s*-*s*-HPMA) nanogels were summarized in **Table 1**. All the nanogels displayed narrow size distributions with PI < 0.1 and good stability (Figure S1, Supporting Information). The D_h of P(VCL-*s*-*s*-HPMA) nanogels increased from 89 to 196 nm when the feeding amount of HPMA increased

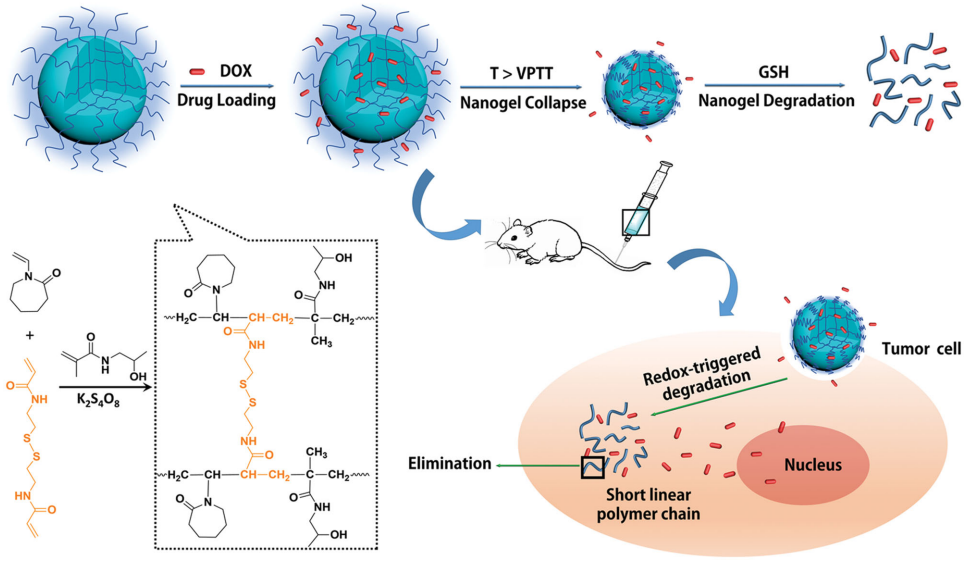

Scheme 1. Schematic representation of the preparation, temperature and redox sensitivity of PVCL-based biodegradable nanogels with fast intracellular drug release for effective antitumor drug delivery.

Part. Part. Syst. Charact. **2015**,
DOI: 10.1002/ppsc.201500153

Table 1. The recipes and colloidal data of nanogels.

Sample	VCL [mg]	HPMA [mg]	D_h[b] [nm]	PI[c]	Zeta potential[d] [mv]	VPTT[e] [°C]
P(VCL-*s*-*s*-HPMA-0)[a]	500	0	89	0.02	−7.3	/
P(VCL-*s*-*s*-HPMA-2)	490	10	102	0.04	−12.7	35.8
P(VCL-*s*-*s*-HPMA-5)	475	25	154	0.01	−15.9	40.2
P(VCL-*s*-*s*-HPMA-8)	460	40	196	0.01	−19.2	44.3

[a]Mass fraction (%) of HPMA to the total weight of monomers; [b]Measured in phosphate buffer (pH 7.4) at 25 °C by DLS; [c]Polydispersity index of the particle size; [d]Determined in phosphate buffer at pH 7.4 at 25 °C; [e]Determined in phosphate buffer at pH 7.4.

from 0 to 8 wt%. With more hydrophilic HPMA introduced in, the nanogels swelled more significantly, giving rise to the larger D_h.[23] Transmission electron microscopy (TEM) images of P(VCL-*s*-*s*-HPMA) nanogels with different HPMA mass fraction were shown in **Figure 1**A–C, and all the nanogels displayed a uniform and spherical morphology. With the increase in the feeding amounts of HPMA from 2 to 8 wt%, diameter of the P(VCL-*s*-*s*-HPMA) nanogels increased from 60 ± 10 to 95 ± 10 nm, which is consistent with the D_h order measured by dynamic scattering light (DLS). It should be noted that the D_h is much larger than that obtained from TEM, suggesting that the nanogels are highly swelled in aqueous medium, which ensured the higher stability and loading capacity of nanohydrogels. In the FTIR spectrum of P(VCL-*s*-*s*-HPMA-5) nanogels (Figure S2, Supporting Information), the peaks appearing at 1630 and 1481 cm^{-1} were attributed to amide I band and C-N belonged to the characteristic peaks of PVCL.[24] The characteristic peaks of HPMA at 1535 cm^{-1} could be clearly observed,[25] which demonstrated that the comonomer HPMA was successfully introduced into the polymer networks.

The temperature-sensitivity of nanogels was investigated through tracing the D_h and scattered light intensity of the samples under a heating process. The D_h of all the samples decreased as temperature increased from 20 to 65 °C (Figure 1D–F), which corresponds to the sharp volume phase transition of PVCL-based hydrogel.[26] For details, the D_h of P(VCL-*s*-*s*-HPMA-8), having the HPMA feeding amount of 8%, decreased from 196 to 116 nm with temperature increasing from 20 to 65 °C. The distinct shrinkage of P(VCL-*s*-*s*-HPMA) nanogels offers possibilities for the nanogels to pump the drugs out.[9a] The VPTT, at which polymer networks undergo a dramatically volume collapse, was calculated from the D_h versus T curves for each nanogel. The VPTT of P(VCL-*s*-*s*-HPMA-2), P(VCL-*s*-*s*-HPMA-5), and P(VCL-*s*-*s*-HPMA-8) is 35.8, 40.2, and 44.3 °C, respectively, which shifted to higher temperature when the content of HPMA increased, owing to the fact that more HPMA incorporated in the polymer networks would improve their hydrophilicity and made it need higher temperature to break the balance of hydrophilic and hydrophobic interaction.[23,27] In addition, with increasing temperature, an abrupt increase of the scattered light intensity was observed for each nanogel at the temperature around their VPTT, which was consistent with the volume collapse and indicated the hydrophilic/hydrophobic transition of nanogels. To trigger drug release in

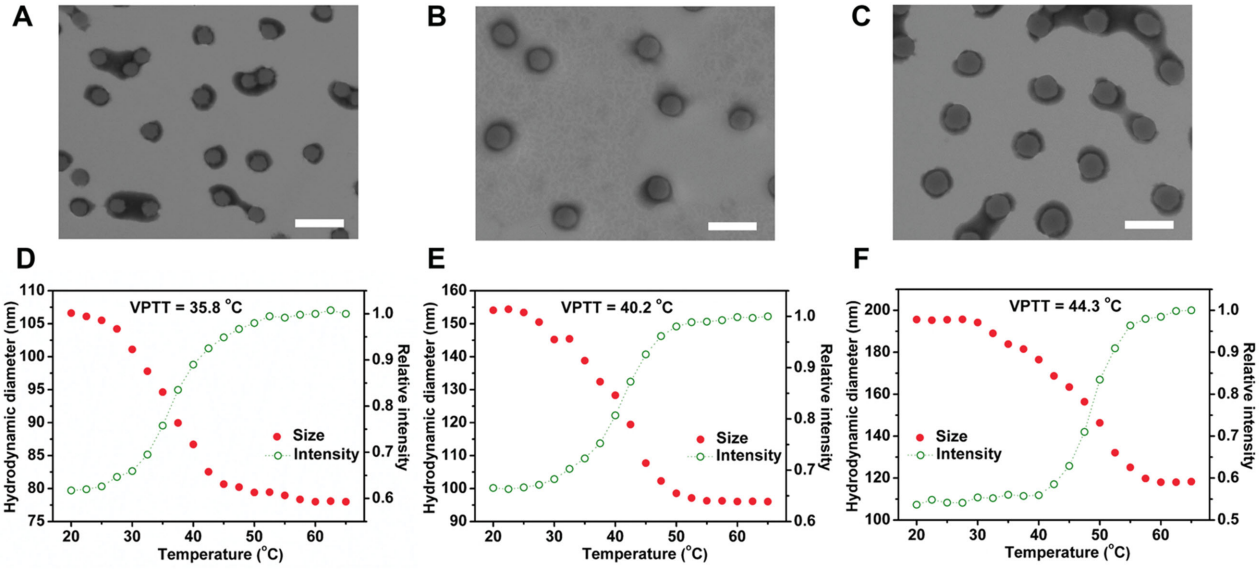

Figure 1. TEM images of A) P(VCL-*s*-*s*-HPMA-2), B) P(VCL-*s*-*s*-HPMA-5), and C) P(VCL-*s*-*s*-HPMA-8) nanogels. The scale bars are 200 nm. Size and scattered light intensity change of D) P(VCL-*s*-*s*-HPMA-2), E) P(VCL-*s*-*s*-HPMA-5), and F) P(VCL-*s*-*s*-HPMA-8) nanogels in phosphate buffer of pH 7.4 as a function of temperature.

tumor tissue, where the local temperature is usually higher than normal tissue, while avoiding the premature drug leakage during blood circulation, P(VCL-*s*-*s*-HPMA-5) nanogel that owning a VPTT (40.2 °C) slightly above normothermia is desirable and chosen as example for further study.

2.2. Redox Degradation of P(VCL-*s*-*s*-HPMA) Nanogels

The incorporation of cleavable crosslinker BAC offers reduction-triggered degradability to the nanogels. The degradation property of the nanogels was investigated by tracing the change of turbidity in response to reductive agent GSH. Degradation of cleavable cross-linking points in the polymer networks would lead to the nanogel deconstruction and thereafter the turbidity of samples decrease, which could be monitored by DLS. **Figure 2**A showed the turbidity trend of P(VCL-*s*-*s*-HPMA-5) nanogels in the presence of GSH with different concentrations at 37 °C. In the absence of GSH, the relative turbidity of P(VCL-*s*-*s*-HPMA-5) nanogels was retained at 100% after 12 h incubation in phosphate buffer at pH 7.4, suggesting that the nanogels were stable under physiological conditions. It can be observed that the relative turbidity of P(VCL-*s*-*s*-HPMA-5) nanogels rapidly decreases to zero within 4 h in the presence of 20×10^{-3} M GSH, which indicates the disassembly of nanogels resulted from the cleavage of disulfide bond. When incubated with a lower concentration of GSH (10×10^{-3} M), it takes »12 h to get a complete degradation of the nanogels. This suggested that high concentration of GSH would accelerate the degradation rate of nanogels in which more disulfide bonds were cleaved via thiol-disulfide exchange reaction at higher GSH concentration.[16b]

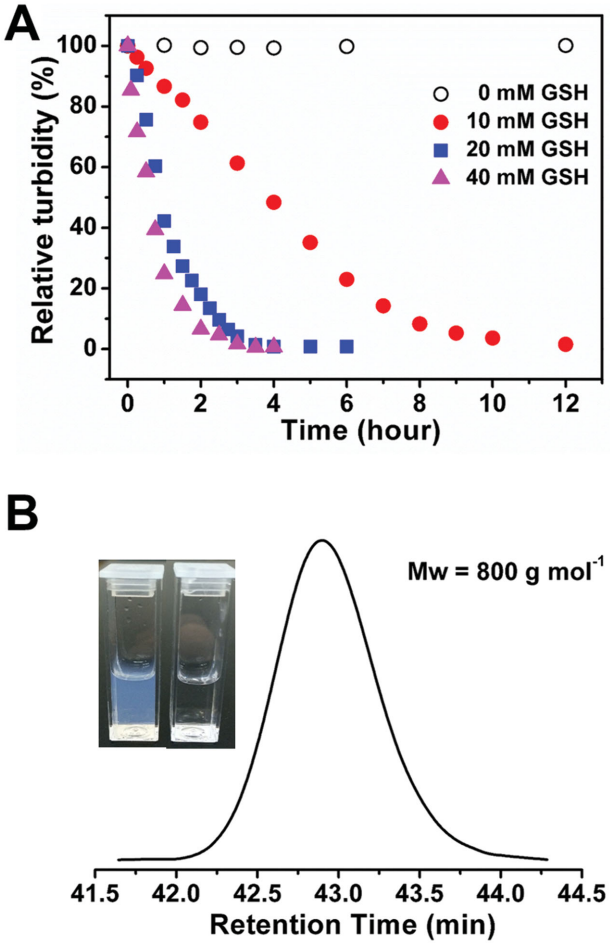

Figure 2. Investigations on the redox degradation of P(VCL-*s*-*s*-HPMA-5) nanogels: A) the change of relative turbidity of P(VCL-*s*-*s*-HPMA-5) nanogels in the presence of different concentration of GSH at 37 °C. B) GPC trace of the polymer chain of nanogels degraded in 10×10^{-3} M GSH. Inset: Photographs of nanogels before (left) and after (right) degradation in the presence of 10×10^{-3} M GSH for 12 h.

A further analysis of the degraded products, which was carried on by gel permeation chromatography (GPC) measurements (Figure 2B), showed the degraded polymer had a low molecular weight (800 g mol^{-1}). The inset photographs showed that the nanogels before degradation presented an opaque emulsion, in which course they turned into a transparent solution after a 12 h of incubation in 10×10^{-3} M GSH, suggesting the complete cleavage of disulfide bond and the disassembly of nanogels. The deconstruction of nanogels into short polymer chains, which could be easily eliminated from the body through the excretion pathway, can bring about reduced cytotoxicity of the materials.[28] The above results demonstrated that the disulfide-crosslinked P(VCL-*s*-*s*-HPMA) nanogels are highly sensitive to reductive condition. The degradation of nanogels in reductive environment, like intracellular space of tumor cells, is expected to efficiently trigger the payload release.

2.3. In Vitro Drug Release

Doxorubicin (DOX) was chosen as a model anticancer drug to investigate the potential ability of nanogels to rapidly release the loaded drugs under hyperthermia and reductive condition. The P(VCL-*s*-*s*-HPMA-5) nanogel has a DOX loading of 12.7% when it was incubated with DOX solution at a mass ratio of 0.3 between DOX and nanogels. The effective drug loading of nanogels may be attributed to the hydrophobic interaction and hydrogen bonding interaction between DOX and polymer.[29] TEM images of DOX-loaded nanogels (DOX-NGs) indicated that they maintained a uniform spherical morphology and homogeneous size distribution after drug loading (**Figure 3**A).

The release profiles of DOX in phosphate buffer (pH 7.4) with different concentrations of GSH under normothermia (37 °C) or hyperthermia (41 °C) are shown in Figure 3B. In control experiments conducted at 37 °C, the assay detected only a 15.0% release of DOX in 48 h, suggesting DOX can be well retained in the nanocarriers during the circulation in blood. When incubated at 41 °C that is just higher than the VPTT of P(VCL-*s*-*s*-HPMA-5) nanogels (40.2 °C), the release amount of drug in 48 h increased to 32.0%, which was over two times higher than that at 37 °C. To carefully evaluate the temperature-dependent drug release, the fluorescence emission of the release medium of DOX-NGs at 37 or 41 °C was monitored in real-time (Figure S3, Supporting Information). The DOX fluorescence intensity was quite weak within 6 h at 37 °C, whereas it was significantly intensified when incubated at 41 °C. It suggested the polymer network was in the swelled state at 37 °C holding drugs steadily entrapped in nanogels.

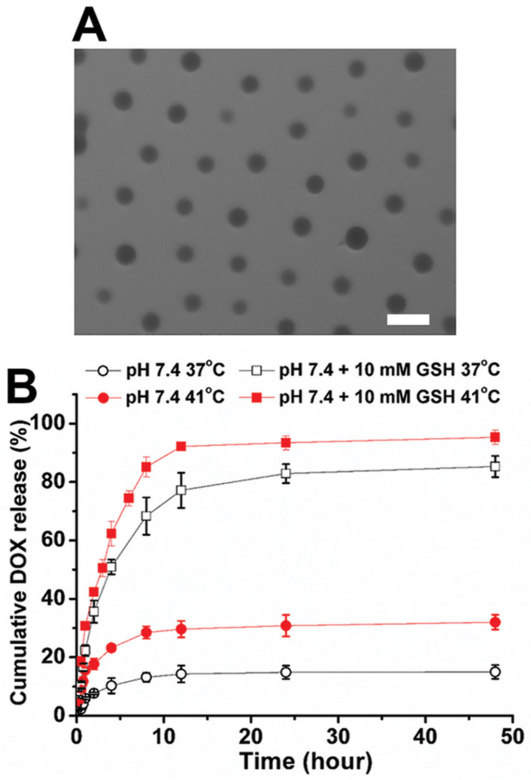

Figure 3. A) TEM image of DOX-NGs (scale bar, 200 nm). B) DOX release profiles of DOX-NGs in 7.4 phosphate buffer at 37 °C (○) and 41 °C (●), and in 7.4 phosphate buffer with 10×10^{-3} M GSH at 37 °C (□) and 41 °C (■).

When temperature rises up to its VPTT, the network undergoes a sharp volume collapse, promoting the release of DOX due to the shortened diffusion distance.[14]

As intracellular GSH concentration is ≈$2–10 \times 10^{-3}$ M,[17] we mimicked the redox environment in the cytosol by addition of 10×10^{-3} M GSH to evaluate the combination effect of reductive condition and temperature on the drug release. At 37 °C, the cumulative release of DOX reached up to 85.3% in 48 h, indicated that the disassembly of nanogels greatly facilitated the drug release. Furthermore, a burst release of DOX under hyperthermia was detected, which led up to 92.2% within 12 h (Figure 3B). The most prominent release of DOX was observed in reductive environment combining with hyperthermia, which was very similar to the tumor microenvironment. It strongly suggested the capability of nanogel to release cargoes after internalization by tumor cells with minimum premature leakage during blood circulation.

2.4. Cellular Uptake

To investigate the effects of hyperthermia on intracellular uptake of nanogels, the human lung adenocarcinoma epithelial A549 cells were incubated with fluorescein-5-maleimide-labeled nanogels (Flu-NGs) under normothermia (37 °C) or low hyperthermia (41 °C) for confocal laser scanning microscopy (CLSM) observation. As shown in **Figure 4**A, a weak green fluorescence can be observed from A549 cells after incubation with Flu-NGs under hyperthermia for 0.5 h, while no obvious fluorescence was observed when cells were treated under normothermia. After 2 h incubation, a prominent green fluorescence was observed from the hyperthermia group, which was stronger than that of the normothermia group, suggesting the greater cellular uptake.

Quantitative analysis of cellular uptake under the two temperatures was performed using flow cytometry. A549 cells treated with Flu-NGs under hyperthermia for 2 h showed a clearly right shift upon cytometric analysis, suggested the cellular uptake of nanogels was accelerated by hyperthermia (Figure 4B). The mean fluorescence intensity of A549 cells incubated at 41 °C for 2 h was over two times higher than that of cells incubated at 37 °C (Figure 4C), indicating that a low hyperthermia could significantly facilitate the intracellular uptake of nanogels as well as improve the targeting efficacy. The enhancement of intracellular may result from the hydrophilic/hydrophobic transition of PVCL chains that intensified the hydrophobic interactions between the nanogels and the cell membranes.[8,10a]

2.5. Intracellular Drug Release and Cytotoxicity

To further confirm the redox- and temperature-triggered drug release in cancer cells, A549 cells were incubated with DOX-NGs (with equivalent DOX concentration of 5 μg mL^{-1}) under normothermia or hyperthermia condition. As shown in **Figure 5**, strong red fluorescence was observed throughout the cell cytoplasm for the hyperthermia group after 2 h incubation, and it can also be seen in a few of cell nucleus, suggesting that DOX was transported into tumor cells, including into the nucleus. For the normothermia group, the red fluorescence was relatively weak and can only be observed in the cytoplasm. These results suggested that DOX-NGs are capable to release encapsulated drugs upon entering tumor cells, and the enhanced drug delivery efficiency and accelerated drug release were found under hyperthermia.

The cytotoxicity of blank nanogels was estimated using MTT assay. As shown in **Figure 6**A, negligible cytotoxicity of blank nanogels at a wide concentration range of 1–500 μg mL^{-1} was detected, suggesting good biocompatibility of the blank nanogels. The cell viability of A549 cells after exposing to DOX-NGs was reduced in a dose-responsive manner (Figure 6B). Notably, the 50% cell inhibition (IC_{50}) value of the DOX-NGs with a short-term low hyperthermia was determined to be 0.50 μg mL^{-1}, which was much lower than that in the absence of hyperthermia (1.58 μg mL^{-1}). The cell viability of free DOX showed a slightly decrease of IC_{50} value after hyperthermia treatment (from 1.55 to 1.08 μg mL^{-1}). The stained images of living cells after different treatments confirmed that the cell viability was not affected by treating with a short-term hyperthermia alone and was consistent with previous studies,[30] but remarkably decreased when treated with DOX-NGs under hyperthermia (Figure S4, Supporting Information). The great improvement of the cytotoxicity of DOX-NGs by combining with a low hyperthermia should be attributed to the enhanced cellular uptake of nanogels as well as the accelerated drug

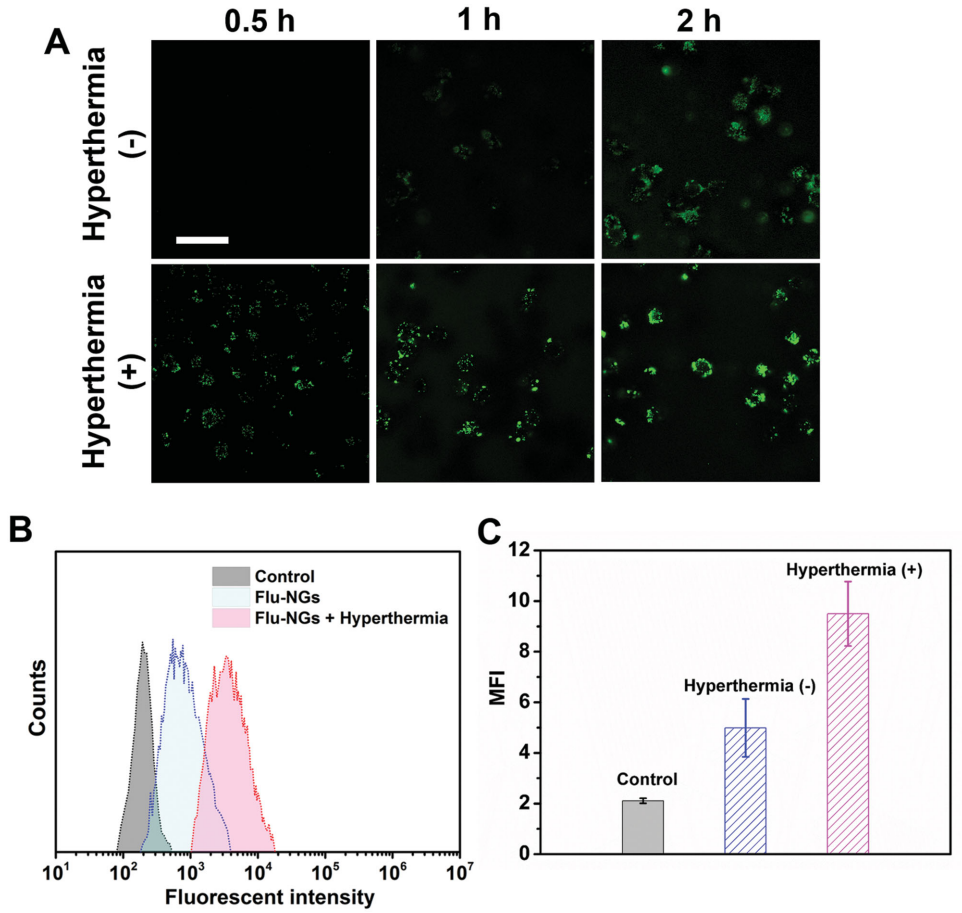

Figure 4. A) Fluorescence images of A549 cells treated with Flu-NGs at 37 or 41 °C for 0.5, 1, and 2 h. The scale bar is 50 μm and corresponds to all the images. B) Flow cytometry analysis of A549 cells treated with Flu-NGs at 37 or 41 °C. C) Mean fluorescence intensity of A549 cells treated with Flu-NGs at 37 or 41 °C after 2 h incubation.

release under hyperthermia, which substantially increased the local concentration of DOX at the target site. Cells treated with free DOX upon hyperthermia also emerged a little decrease in cell viability, which may resulted from improved tissue oxygenation, vascular permeability, and increased tumor cell sensitivity.[31]

2.6. In Vivo Therapy

The passive targeting performance of the nanogel was studied firstly. A549 tumor-bearing mice were intravenously injected with pure near-infrared fluorescence (NIRF) dye Cy7.5 and Cy7.5-labeled nanogels (NG-Cy7.5) at an equimolar dosage of Cy7.5 (50 μg mL^{-1}, 100 μL). The NIRF images were both acquired at 1 and 24 h post injection as shown in **Figure 7**A. The free dye shows no significant tumor enrichment and quick elimination. For NG-Cy7.5, the NIRF signal was observed throughout the whole body with a maximum at the tumor site at 1 h post injection, and the nanogels remain accumulated at tumor site after 24 h injection, suggesting the long circulation of nanogel carriers in bloodstream and accumulation in tumor tissues. This could be attributed to the passive targeting effect of nanogels (with size dimension in the range of 10–200 nm) via enhance permeability and retention effect.[32]

Encouraged by the effective tumor cell killing ability of DOX-NGs in vitro, a tumor therapy treatment study in vivo was performed next. Here, A549 tumor-bearing mice were established by subcutaneous injection of A549 cells into the flank region. When the tumors grew up to ≈5.0 mm in longest dimension, the mice were randomized into three groups ($n = 4$ per group): phosphate buffer saline (PBS), free DOX (3 mg kg^{-1}), and DOX-NGs (25 mg kg^{-1} nanogels, with an equivalent DOX dosage of 3 mg kg^{-1}). The mice were dosed three times at day 0, day 2, and day 4, respectively. There was no statistical difference among group mean tumor volumes at the onset of treatment ($P > 0.05$). The tumor sizes of different treatment groups were measured every 2 d, as shown in Figure 7B. The tumors of PBS group enlarged rapidly and the size of which increased over 30 times after 15 d. As for the free DOX group, an obvious increase of tumor size can also be observed, while its increase amount was obviously less than that of the PBS group because of the anti-tumor effect of DOX. Impressively, a pronounced restraint of tumor size with statistically significant difference was observed in mice treated with DOX-NGs with $P < 0.05$, where the mean

Part. Part. Syst. Charact. **2015**,
DOI: 10.1002/ppsc.201500153

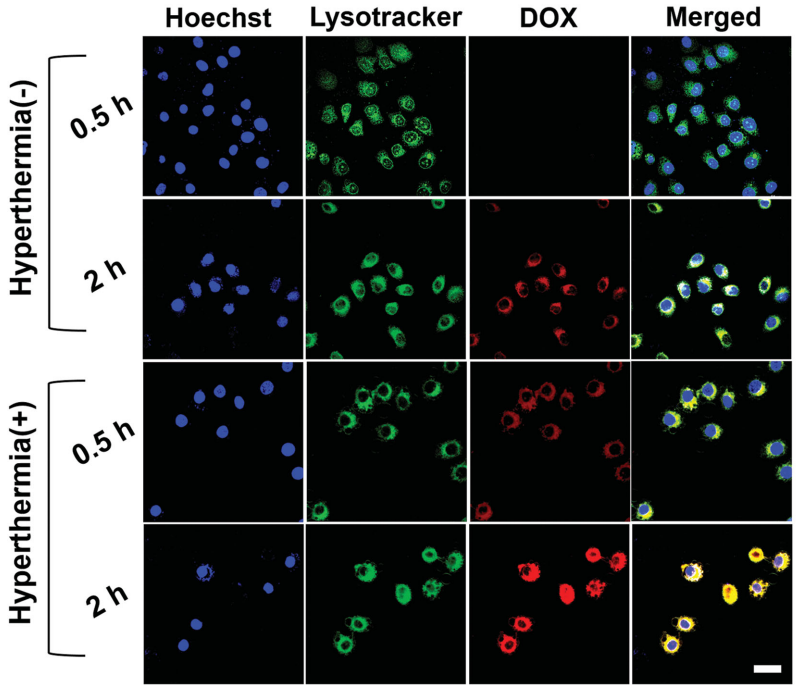

Figure 5. CLSM images of A549 cells incubated with DOX-NGs under normothermia or hyperthermia for 0.5 and 2 h (scale bar, 25 μm). The nucleus and lysosomes of A549 cells were stained with Hoechst (blue) and Lysotracker Green (green), respectively.

tumor volume was reduced from 1111.6 mm^3 in control group to 224.7 mm^3 ($P = 0.0287$). At the 15th day, all the mice were euthanized, tumors were excised and weighted (Figure 7C,D). The weights of tumors for PBS group, free DOX group, and DOX-NGs group were 0.9330 ± 0.1398, 0.7852 ± 0.1398, and 0.4192 ± 0.0939 g, respectively. Clearly, the antitumor efficiency of DOX-NGs group was significantly superior to the other two groups ($P < 0.01$), displaying an inhibition rate of 55.1% and 46.6% compared with PBS and free DOX groups, respectively. The remarkable antitumor efficiency of DOX-NGs in comparison with free drugs suggested the selective drug delivery and efficient drug release of nanogel, which demonstrated its potential as drug delivery carrier.

The body weight of mice was simultaneously measured following the treatments, since the change of which can be seen as an indicator of systemic toxicity (Figure S5, Supporting Information). The body weight of DOX-NGs group stayed the same during the entire experimental period, suggesting no severe systemic toxicity of DOX-NGs. Histological analysis of hematoxylin-eosin (H&E) staining indicated that both PBS and DOX-NGs groups exhibited no obvious differences in tissues including the heart, liver, spleen, and kidney (Figure S6, Supporting Information). On the contrary, the heart slice of free DOX group presented myocardial fiber rupture, which was attributed to the cardiactoxicity of DOX. The safety of nanogels in vivo was further investigated via immunohistochemical assay (Figure S7, Supporting Information). The mice treated with nanogels were sacrificed by cervical dislocation and the tissues including the brain, heart, liver, spleen, lung, and kidney were collected for CD68 immunohistochemical staining to evaluate the acute inflammatory reaction. No inflammatory reaction was observed in all tissues, indicating the outstanding safety of nanogels for in vivo application.

3. Conclusion

In summary, a new type of dual-responsive P(VCL-*s*-*s*-HPMA) nanogels with finely tunable VPTT and excellent redox-labile property were prepared. The nanogels keep hydrophilic and swelled at 37 °C that ensured the stable and long blood circulation, whereas undergo sharp hydrophilic/hydrophobic transition and volume collapse under hyperthermia (41 °C) which enhanced the cellular uptake and drug release at tumor site. Owing to the incorporation of disulfide bond, the nanogels can efficiently disassemble into short polymer chains (≈800 Da) in the presence of 10×10^{-3} M GSH. The drug-loaded nanogels are stable in physiological conditions with low leakage of DOX (15% in 48 h), while it allows a burst release of DOX (≈92% in 12 h) in the presence of 10×10^{-3} M GSH under hyperthermia. The greater cellular uptake and accelerated drug release against A549 cells under hyperthermia were observed. The cell viability assays showed highly improved cell killing efficiency of DOX-NGs under hyperthermia, where the IC_{50} value (0.5 μg mL^{-1}) is much lower than that under normothermia (1.58 μg mL^{-1}). In vivo studies showed that the DOX-NGs can significantly restrain the growth of tumor and no side effects to normal tissues were observed. The above results demonstrated the great potential of the dual-responsive biodegradable nanogels for cancer therapy, and we believe they may also be desirable for the combination treatment of thermal therapy and chemotherapy in clinical application to improve treatment.

4. Experimental Section

Materials: *N*-vinylcaprolactam (VCL) (99%) was obtained from Tokyo Chemical Industry. HPMA was synthesized as described in a recent report.[33] BAC was purchased from Sigma-Aldrich and used without further purification. Sodium bicarbonate ($NaHCO_3$), sodium dodecyl sulfate (SDS), and potassium persulfate (KPS) were purchased from Shanghai Chemical Reagents Company. KPS was recrystallized from water. GSH and Tris(2-carboxyethyl)phosphine hydrochloride (TCEP) were purchased from Shanghai Aladdin Chemistry Co., Ltd. DOX hydrochloride was purchased from Beijing Huafeng United Technology Company. 3-(4,5-dimethylthiazol-2-yl)-2,5-diphenyltetrazolium bromide (MTT) and other biological reagents were obtained from Sigma-Aldrich. Fluorescein-5-maleimide and NIRF dye Cy7.5 maleimide was purchased from Shanghai Seebio Biotech, Inc. Hoechst 33258, Lysotracker Green and Calcein-AM were purchased from KeyGen Biotech, Inc. (Nanjing). The other chemicals were analytical reagents and used as received.

Preparation of Disulfide-Crosslinked P(VCL-s-s-HPMA) Nanogels: Disulfide-crosslinked nanogels were prepared by aqueous precipitation polymerization approach, and denoted as P(VCL-*s*-*s*-HPMA). In a typical procedure, 475 mg of VCL, 25 mg of HPMA, together with 20.0 mg (4 wt% to the monomers) of BAC, 10.0 mg (2 wt%) of SDS and

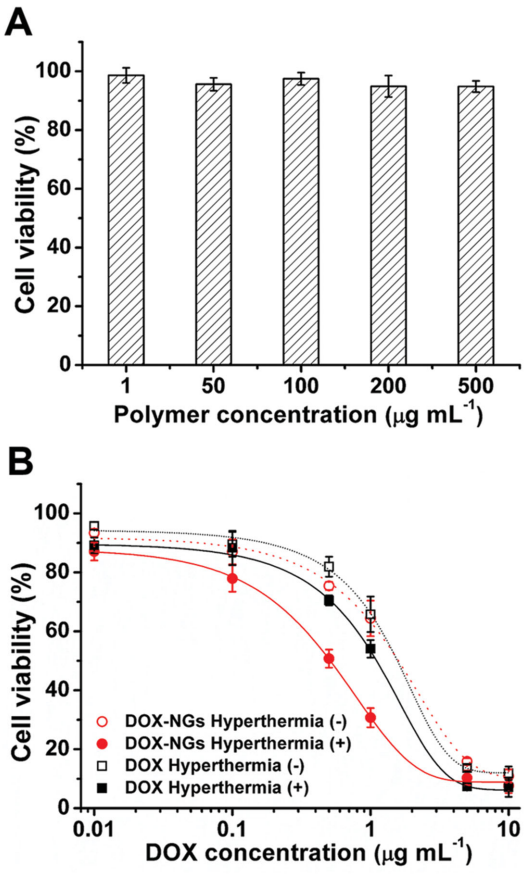

Figure 6. A) Cell viability of A549 cells exposed to blank nanogels for 48 h. B) Cell viability of A549 cells treated with free DOX and DOX-NGs in the presence or absence of hyperthermia for 48 h. Means and standard errors are shown.

12.5 mg (2.5 wt%) of $NaHCO_3$ were dissolved in 100.0 g of deionized water, to a final total monomer concentration of 0.5 wt%. The mixture was heated to 70 °C and purged with nitrogen. After mechanical stirring for 1 h, an aqueous solution of KPS (12.5 mg in 1 mL deionized water) was added into the system. The mixture was allowed to stir at 70 °C under a nitrogen atmosphere for 6 h, and then cooled to room temperature. After the polymerization, the obtained nanogels were washed three times with deionized water (sedimentation: 25 000 rpm for 10 min). The mass fraction of HPMA to total monomers was varied from 0% up to 8% to obtain a series of P(VCL-*s*-*s*-HPMA) nanogels with different VPTT (Table 1). For TEM observation, the nanogels were negative stained with 1% phosphotungstic acid, excepting the DOX-loaded one.

Thermosensitivity Study of Nanogels: The thermosensitivity of the family of P(VCL-*s*-*s*-HPMA) nanogels was investigated by DLS measurement. The nanogels were dispersed in phosphate buffer of pH 7.4 and the change of hydrodynamic diameters was monitored as a function of HPMA content with increasing temperature from 20 to 65 °C. The stabilization time between each measurement was 300 s.

Redox Degradation of Nanogels: The change of turbidity and hydrodynamic diameter of nanogels were monitored by DLS measurement. P(VCL-*s*-*s*-HPMA-5) nanogels with an identical concentration of 1.0 mg mL^{-1} were incubated in pH 7.4 phosphate buffers containing GSH with various concentrations at 37 °C for degradation. At predetermined intervals, the particle size and scattering intensity of the samples were measured. The relative turbidity was calculated as the ratio of the scattering intensity at each interval to the initial scattering intensity of the samples. The average molecular weight of the degraded polymer chains was estimated by GPC measurement.

Drug Loading and Release In Vitro: DOX was chosen as a model anticancer drug to study the drug loading and release profiles of the P(VCL-*s*-*s*-HPMA) nanogels. In a typical procedure, 3 mg of DOX was dissolved in deionized water, to a concentration of 1 mg mL^{-1}, and the pH of the solution was adjusted to 8.0 with 0.1 M NaOH. After that, 10 mg of P(VCL-*s*-*s*-HPMA-5) nanogels were dispersed in the above DOX aqueous solution, and stirred at room temperature for 24 h. The suspension was centrifuged (25 000 rpm, 10 min) and washed with deionized water twice to remove the unloaded DOX. All the supernatant was collected for calculating the drug loading efficiency by UV–vis spectrometry at the wavelength of 480 nm. The drug loading content (LC) and encapsulation efficiency (EE) were expressed according to the following formulas: LC (%) = (weight of loaded drug)/(total weight of nanogels); EE (%) = (weight of loaded drug)/(weight of initially added drug).

To investigate the drug release behavior in vitro, DOX-NGs were dispersed in 1 mL of pH 7.4 phosphate buffer with or without GSH (10×10^{-3} M) and placed in a dialysis bag (molecular weight cutoff 14 000 Da), which was submerged into 100 mL of corresponding buffer. The release experiments were performed at 37 or 41 °C under constant shaking. At desired time intervals, 2 mL of external buffer was taken out for UV–vis spectra analysis, and replenished with an equal volume of fresh medium. The released drug was calculated as the ratio of the amount of drug estimated in the releasing medium to the total amount of drug loaded in the nanogels. All DOX release data were averaged with three measurements.

Cellular Uptake: To observe the cellular uptake, fluorescein-5-maleimide-labeled nanogels (Flu-NGs) were prepared. Briefly, P(VCL-*s*-*s*-HPMA-5) nanogels (25 mg) were stirred with a slight amount of TCEP for 12 h resulting in partial reduction of disulfide bond to generate free thiol. The thiol-modified nanogels were stirred with 5 mg fluorescein-5-maleimide for 24 h under nitrogen atmosphere to fabricate Flu-NGs via thiol-maleimide coupling reaction.

Human lung adenocarcinoma epithelial cell (A549 cells, 1×10^4 cells per well) were seeded into 6-well plates and allowed to attach overnight. Then, the cells were treated with Flu-NGs (at a final polymer content of 50 μg mL^{-1}) at the temperature below (37 °C) or above (41 °C) the VPTT of nanogels for 0.5, 1, and 2 h, respectively. The cells were observed by CLSM, and the fluorescence was imaged at λ_{EX} (488 nm).

For quantitative evaluation of the cellular uptake, A549 cells (3×10^4 cells per well) grown in 6-well plates were treated with Flu-NGs at 37 or 41 °C for different time periods (0.5, 1, 2, 3, and 4 h). After being detached with the trypsin solution and resuspended in PBS, the intensity of cellular fluorescence was determined on a Gallios flow cytometry.

Intracellular Drug Release: A549 cells were seeded in culture dishes at a density of 1×10^4 cells and allowed to attach overnight. The cells were treated with DOX-NGs (the final DOX concentration was 5 μg mL^{-1}) at 37 or 41 °C for different time periods (0.5 and 2 h), washed with PBS, stained with Hoechst 33258 for cell nuclei and Lysotracker Green for lysosomes, and then observed by CLSM. Hoechst 33258, Lysotracker Green, and DOX were excited at 352, 504, and 488 nm, respectively, and the emission wavelengths are 455, 511, and 595 nm, respectively.

Cytotoxicity: Cytotoxicity of DOX-NGs and blank nanogels were evaluated by quantification of apoptotic A549 cells. A549 cells were seeded in a 96-well plate at a density of 8×10^3 cells per well and cultured overnight. Cells were incubated with blank nanogels, DOX-NGs or free DOX at a series of concentration for 48 h at 37 °C. The hyperthermia group was incubated at 41°C for 2 h, followed by incubation at 37 °C for 46 h. Next, the cells were washed with PBS and incubated in 20 μL of MTT solution (5 mg mL^{-1} in PBS) for an additional 4 h. After the removal of the supernatant, 150 μL of dimethysulfoxide (DMSO) was added to each well to dissolve the formazan crystals. After 15 min of gentle shaking in darkness, the optical density was determined at 490 nm using a microplate reader. Cell viability was calculated in reference to cells incubated with culture medium alone. Each data point was averaged from five measurements.

In Vivo NIRF Imaging: To observe the in vivo distribution of nanogels, NIRF dye Cy7.5-labeled nanogels (NG-Cy7.5) were prepared following

Part. Part. Syst. Charact. **2015**,
DOI: 10.1002/ppsc.201500153

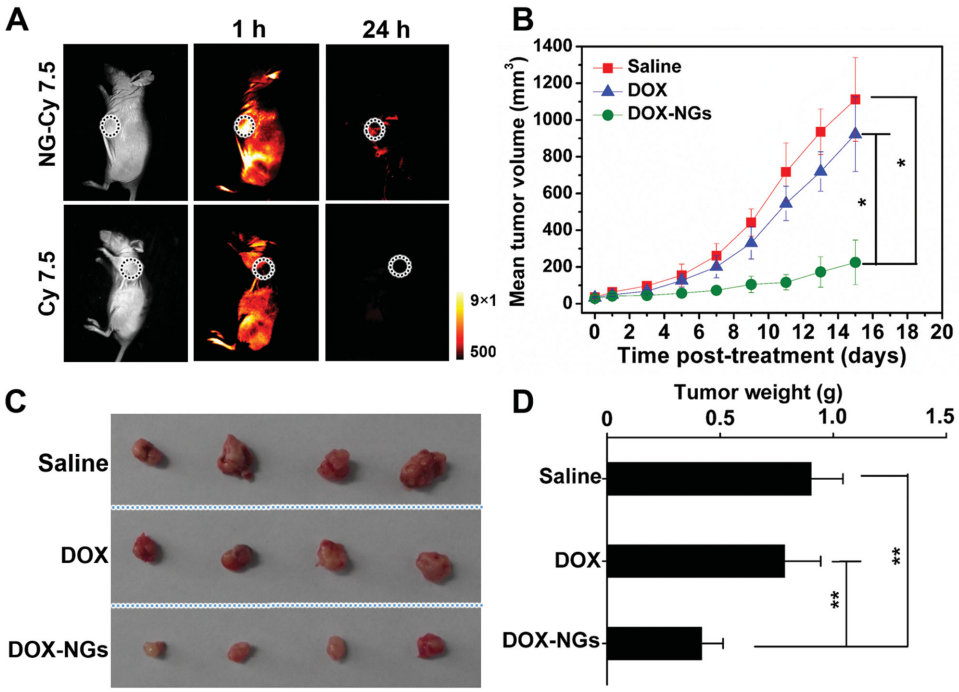

Figure 7. A) In vivo NIRF imaging of pure NIRF dye (Cy7.5), and NG-Cy7.5 in tumor-bearing mice (marked with circle) at 1 and 24 h post injection. B) Tumor growth curves of different groups after treatment. Tumor sizes were measured every 2 d. The groups of PBS, free DOX, and DOX-NGs were statistically identical. The antitumor efficiency of DOX-NGs was particularly prominent and was superior to all the other groups ($P < 0.05$). C) Photograph of tumors after excision from PBS, free DOX, and DOX-NGs groups after treatment. D) Tumor weights of each group. Means and standard errors are shown. *$P < 0.05$ and **$P < 0.01$.

the same procedure to fabricate Flu-NGs. The tumor-bearing mice were intraperitoneally injected with NG-Cy7.5 at a dose of 20 mg kg^{-1}. In control group, pure Cy7.5 with equimolar amounts of Cy7.5 (50 μg mL^{-1}) was intraperitoneally injected into the mice. NIRF imaging was performed using In Vivo Xtreme (Bruker, USA) at 1 and 24 h post injection. All fluorescence images were acquired using a single-filter set (E_x 760 nm, E_m 790 nm) with a 10 s exposure time.

In Vivo Therapy: Tumor-bearing mice (with tumor size measured ≈5.0 mm in the longest dimension) were randomized into three treatment groups ($n = 4$ per group): PBS (Group I), free DOX (3 mg kg^{-1}, Group II), DOX-NGs (25 mg kg^{-1} nanogels, with an equivalent DOX dosage of 3 mg kg^{-1}, Group III). The mice were dosed three times after 0 d, 2 d, and 4d, respectively, administered through the tail veins. All mice were maintained in the animal house after treatment, and the tumor volumes were monitored every 2 d by digital caliper measurements. The tumor volume was calculated by the formula $V = 1/2(LW^2)$, where L is the length (longest dimension) and W is the width (shortest dimension). At the 15th day, all the animals were euthanized, and the tumors were dissected and weighed. All animal experiments were carried out in accordance with guidelines evaluated and approved by the ethics committee of Fudan University.

Statistical Analysis: An unpaired student's *t*-test was used for comparison between two testing groups. A probability (P) less than 0.05 was considered statistically significant. All data in this paper are expressed as mean ± standard deviation unless otherwise indicated.

Supporting Information

Supporting Information is available from the Wiley Online Library or from the author.

Acknowledgements

The authors are grateful for the support of the National Science Foundation of China (Grant Nos. 51273047 and 51473037) and the "Shu Guang" project (12SG07) supported by Shanghai Municipal Education Commission and Shanghai Education Development Foundation.

Received: August 14, 2015
Revised: September 22, 2015
Published online:

[1] S. Mura, J. Nicolas, P. Couvreur, *Nat. Mater.* **2013**, *12*, 991.
[2] a) T. M. Allen, P. R. Cullis, *Science* **2004**, *303*, 1818; b) D. Peer, J. M. Karp, S. Hong, O. C. FaroKhzad, R. Margalit, R. Langer, *Nat. Nanotechnol.* **2007**, *2*, 751; c) F. Danhier, O. Feron, V. Preat, *J. Controlled Release* **2010**, *148*, 135.
[3] a) W. Li, J. Li, J. Gao, B. Li, Y. Xia, Y. Meng, Y. Yu, H. Chen, J. Dai, H. Wang, Y. Guo, *Biomaterials* **2011**, *32*, 3832; b) W. Li, L. Huang, X. Ying, Y. Jian, Y. Hong, F. Hu, Y. Du, *Angew. Chem. Int. Ed.* **2015**, *54*, 3126.
[4] X. Guo, C. Shi, G. Yang, J. Wang, Z. Cai, S. Zhou, *Chem. Mater.* **2014**, *26*, 4405.
[5] Y. Pan, Y. Chen, D. Wang, C. Wei, J. Guo, D. Lu, C. Chu, C. Wang, *Biomaterials* **2012**, *33*, 6570.
[6] a) S. Bian, J. Zheng, W. Yang, *J. Polym. Sci., Part A: Polym. Chem.* **2014**, *52*, 1676; b) Y. Tian, J. Zheng, X. Tang, Q. Ren, Y. Wang, W. Yang, *Part. Part. Syst. Charact.* **2015**, *32*, 547.
[7] C. Song, V. Appleyard, K. Murray, T. Frank, W. Sibbett, A. Cuschieri, A. Thompson, *Int. J. Cancer* **2007**, *121*, 1055.
[8] J. Akimoto, M. Nakayama, T. Okano, *J. Controlled Release* **2014**, *193*, 2.
[9] a) J. Liu, A. Debuigne, C. Detrembleur, C. Jerome, *Adv. Healthc. Mater.* **2014**, *3*, 1941; b) L. A. Lyon, Z. Meng, N. Singh, C. D. Sorrell, A. S. John, *Chem. Soc. Rev.* **2009**, *38*, 865.
[10] a) J. Akimoto, M. Nakayama, K. Sakai, T. Okano, *Biomacromolecules* **2009**, *10*, 1331; b) J. Akimoto, M. Nakayama, K. Sakai, T. Okano, *Mol. Pharmaceut.* **2010**, *7*, 926.

[11] a) X. Guo, D. Li, G. Yang, C. Shi, Z. Tang, J. Wang, S. Zhou, *ACS Appl. Mater. Interfaces* **2014**, *6*, 8549; b) J. E. Chung, M. Yokoyama, T. Okano, *J. Controlled Release* **2000**, *65*, 93.
[12] K. Matsuoka, Y. Moroi, *Curr. Opin. Colloid Interface Sci.* **2003**, *8*, 227.
[13] A. V. Kabanov, S. V. Vinogradov, *Angew. Chem. Int. Ed.* **2009**, *48*, 5418.
[14] C. Liu, J. Guo, W. Yang, J. Hu, C. Wang, S. Fu, *J. Mater. Chem.* **2009**, *19*, 4764.
[15] a) B. Chang, D. Chen, Y. Wang, Y. Chen, Y. Jiao, X. Sha, W. Yang, *Chem. Mater.* **2013**, *25*, 574; b) Y. Wang, J. Nie, B. Chang, Y. Sun, W. Yang, *Biomacromolecules* **2013**, *14*, 3034.
[16] a) G. Saito, J. A. Swanson, K. D. Lee, *Adv. Drug Delivery Rev.* **2003**, *55*, 199; b) F. Meng, W. E. Hennink, Z. Zhong, *Biomaterials* **2009**, *30*, 2180.
[17] a) R. Cheng, F. Feng, F. Meng, C. Deng, F. Jan, Z. Zhong, *J. Controlled Release* **2011**, *152*, 2; b) F. Q. Schafer, G. R. Buettner, *Free Radical Biol. Med.* **2001**, *30*, 1191.
[18] a) H. Sun, B. Guo, R. Cheng, F. Meng, H. Liu, Z. Zhong, *Biomaterials* **2009**, *30*, 6358; b) H. Sun, B. Guo, X. Li, R. Cheng, F. Meng, H. Liu, Z. Zhong, *Biomacromolecules* **2010**, *11*, 848.
[19] a) Y. Wang, Y. Yan, J. Cui, L. Hosta-Rigau, J. K. Heath, E. C. Nice, F. Caruso, *Adv. Mater.* **2010**, *22*, 4293; b) A. N. Zelikin, J. F. Quinn, F. Caruso, *Biomacromolecules* **2006**, *7*, 27.
[20] J. C. Gaulding, M. H. Smith, J. S. Hyatt, A. Fernandez-Nieves, L. A. Lyon, *Macromolecules* **2012**, *45*, 39.
[21] S. Nayak, L. A. Lyon, *Angew. Chem. Int. Ed.* **2005**, *44*, 7686.
[22] J. Kopecek, P. Kopeckova, T. Minko, Z. R. Lu, *Eur. J. Pharm. Biopharm.* **2000**, *50*, 61.
[23] E. E. Makhaeva, H. Tenhu, A. R. Khokhlov, *Macromolecules* **2002**, *35*, 1870.
[24] S. Shah, A. Pal, R. Gude, S. Devi, *Eur. Polym. J.* **2010**, *46*, 958.
[25] Y. Pan, D. Li, S. Jin, C. Wei, K. Wu, J. Guo, C. Wang, *Polym. Chem.* **2013**, *4*, 3545.
[26] A. Imaz, J. Forcada, *Eur. Polym. J.* **2009**, *45*, 3164.
[27] A. Imaz, J. Forcada, *J. Polym. Sci., Part A: Polym. Chem.* **2011**, *49*, 3218.
[28] M. Prabaharan, J. J. Grailer, S. Pilla, D. A. Steeber, S. Gong, *Biomaterials* **2009**, *30*, 3009.
[29] a) A. Imaz, J. Forcada, *J. Polym. Sci., Part A: Polym. Chem.* **2010**, *48*, 1173; b) Y. Wang, J. Zheng, Y. Tian, W. Yang, *J. Mater. Chem. B* **2015**, *3*, 5824.
[30] Y. Li, S. Pan, W. Zhang, Z. Du, *Nanotechnology* **2009**, *20*, 065104.
[31] a) C. W. Song, *Cancer Res.* **1984**, *44*, 4721; b) P. M. Krawczyk, B. Eppink, J. Essers, J. Stap, H. Rodermond, H. Odijk, A. Zelensky, C. van Bree, L. J. Stalpers, M. R. Buist, T. Soullie, J. Rens, H. J. M. Verhagen, M. J. O'Connor, N. A. P. Franken, T. L. M. ten Hagen, R. Kanaar, J. A. Aten, *Proc. Natl. Acad. Sci. USA* **2011**, *108*, 9851.
[32] H. Maeda, J. Wu, T. Sawa, Y. Matsumura, K. Hori, *J. Controlled Release* **2000**, *65*, 271.
[33] B. Apostolovic, S. P. E. Deacon, R. Duncan, H. A. Klok, *Biomacromolecules* **2010**, *11*, 1187.

Part. Part. Syst. Charact. **2015**,
DOI: 10.1002/ppsc.201500153